

Motions of a dimer on a periodic potential

Johann Maddi, Christophe Coste, and Michel Saint Jean

*Laboratoire “Matière et Systèmes Complexes” (MSC), UMR 7057 CNRS, Université Paris–Diderot (Paris 7),
75205 Paris Cedex 13, France*



(Received 13 October 2022; accepted 16 November 2022; published 1 December 2022)

A dimer on a periodic potential is a simple system that exhibits a surprisingly rich dynamics. This system is conservative, but it is nonlinear and nonintegrable. In a previous work, we evidenced the autoparametric excitation of the relative motion by the center of mass in two limiting cases (very small or very large initial energy, compared to the external potential depth). We extend these results for arbitrary initial energy. The relevant control parameters are the dimer initial energy and the stiffness of the link between the two particles. In this parameter plane, we build a behavior map which classifies the available dynamical regimes of the dimer. The parameters plane can be separated into domains in which the dimer particles are either trapped in adjacent potential wells, slide along the potential, or exhibit more complex motions in which the particles jumps to farthest well or in which the center-of-mass motion is neither monotonous nor periodic. We discuss the thresholds between these domains.

DOI: [10.1103/PhysRevE.106.064201](https://doi.org/10.1103/PhysRevE.106.064201)

I. INTRODUCTION

Two point particles interacting with an external periodic potential and moving on a line are a toy model of an adatoms cluster moving on a surface [1–3]. Because of the underlying periodic potential, the normal modes of the dimer, center-of-mass motion, and relative motion are coupled nonlinearly so that this seemingly simple system exhibits a surprisingly rich dynamics.

Indeed, in such a conservative system, a resonant energy exchange between two oscillatory modes is possible. Relevant examples are coupled Duffing oscillators [4–7], the swinging spring which may evidence resonant behavior. when the frequencies of the elastic and pendular oscillations are in the ratio 2:1 [8,9], and quasiperiodic oscillations observed in accretion disks of massive neutron stars or black holes [10–13]. Such resonances are called *autoparametric* because there is no external forcing.

These resonances in a nonlinear conservative system are usually difficult to analyze [14]. In a previous paper [15] we have studied a dimer in a periodic potential in two limiting cases, when the initial energy and the stiffness are small enough for the dimer particles to remain trapped in adjacent potential wells and conversely when the initial energy and the stiffness are high enough for the external potential to be a small perturbation, so that the dimer basically slides along the potential with small relative oscillations of the particles. In both cases a small natural parameter appears that allows a perturbative approach. Nevertheless, the dynamics of the dimer is much richer, and we extend our previous work with numerical simulations in which we explore the two-dimensional parameter space defined by the stiffness of the harmonic interaction between the particles and by the initial energy of the dimer. Surprisingly enough, we observe that many features of our perturbation analysis may be extended to parameter

regions in which they should not be accurate. In particular, the autoparametric resonance thresholds are valid on a very large parameter range. We also exhibit new regimes, which are out of reach of our perturbative approach, in which the dimer particles may either jump to nonadjacent potential wells or in which the center of mass motion may be a nonmonotonous sliding along the external potential. All these behavior may be summarized in a behavior map with a quite simple structure.

In Sec. II we describe our system, giving an energetic analysis of this conservative system useful to apprehend and classify its main behavior. We also provide a dynamical analysis which reminds the main results of our previous perturbative approach. In Sec. III we recall the main characteristics of the parametric instability. We summarize the various behavior available to the system for a given initial energy and a given stiffness in a *behavior map*. In the next sections, we put the focus on the trapped motions (Sec. IV), the sliding motions (Sec. V), and eventually the jumping motions (Sec. VI). In Sec. VII we summarize our work.

II. A DIMER IN A PERIODIC POTENTIAL

We consider a dimer in an external periodic potential of period a ,

$$U_{\text{ext}}(x_1, x_2) = U_0 \left(2 - \cos \frac{2\pi x_1}{a} - \cos \frac{2\pi x_2}{a} \right), \quad (1)$$

where x_i is the spatial coordinate of the i th particle ($i = 1, 2$) and $2U_0$ is the potential barrier per particle. The interaction between the particles is described by a harmonic potential of stiffness k for which we assume that the equilibrium length, a , is the same as the period of the external potential,

$$U_{el}(x_1, x_2) = \frac{k}{2}(x_2 - x_1 - a)^2. \quad (2)$$

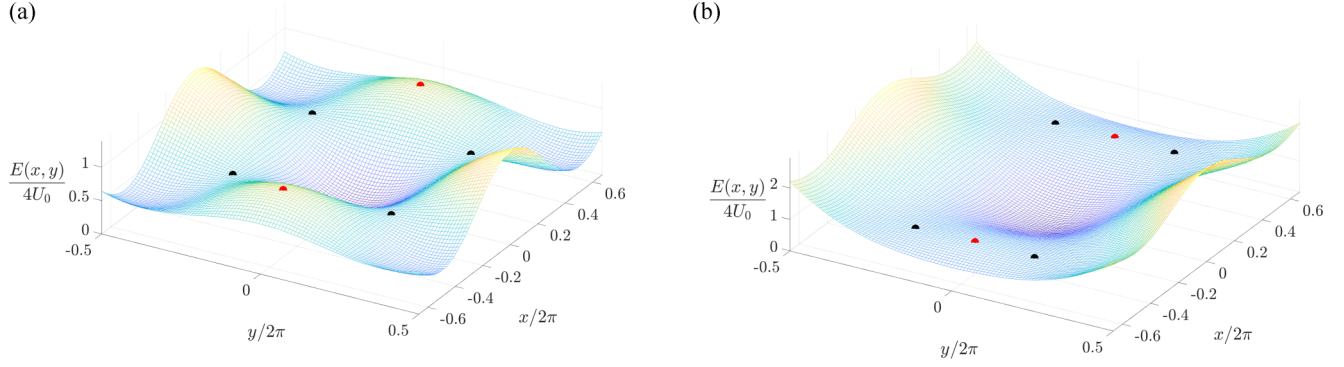


FIG. 1. Potential energy surface for two different stiffnesses. The red dots are the set of maxima $\{(2p + 1)\pi, 0\}$. (a) $K = 0.0792 < K_S$. The black dots are the set of saddle points given by Eq. (10). (b) $K_R > K = 0.3958 > K_S$. The black dots are the set of saddle points given by Eq. (9).

The equations of motion are

$$m\ddot{x}_1 = k(x_2 - x_1 - a) - (2\pi U_0/a) \sin(2\pi x_1/a), \quad (3)$$

$$m\ddot{x}_2 = k(x_1 - x_2 + a) - (2\pi U_0/a) \sin(2\pi x_2/a), \quad (4)$$

where m is the mass of each particle and $\ddot{x}_i \equiv d^2x_i/dt^2$.

We rescale the variables using $a/2\pi$ as the unit length and U_0 as the unit energy, so that $\sqrt{ma^2/4\pi^2U_0}$ is the unit time and $K = ka^2/4\pi^2U_0$ is the dimensionless stiffness. In these units, $U_0 = 1$ but we keep writing it in order to follow the role of the external potential. We introduce the normal modes as

$$x \equiv \frac{x_1 + x_2}{2} - \pi, \quad y \equiv \frac{x_2 - x_1}{2} - \pi, \quad (5)$$

in dimensionless units, where x is the center-of-mass coordinate and y is the relative coordinate (RC). With these variables, the equations of motion become

$$\ddot{x} = -U_0 \sin x \cos y, \quad (6)$$

$$\ddot{y} = -2Ky - U_0 \cos x \sin y. \quad (7)$$

A. Energetic analysis

The dimer in a periodic potential is a conservative system with potential energy

$$E(x, y) = 2U_0(1 - \cos x \cos y) + 2Ky^2. \quad (8)$$

Since U_0 is the energy scale, the two relevant parameters in this energetic analysis are the stiffness K and the mechanical energy E_0 of the dimer. A plot of the potential energy surface as a function of x and y is shown in Fig. 1. An instantaneous state of the dimer is characterized by $(x(t), y(t))$. In order to identify the various dimer behavior that may be encountered, it is convenient to analyze the trajectories of $(x(t), y(t))$ above the potential energy surface according to the values of (E_0, K) .

The potential energy surface has local minima $E_0 = 0$ at the points $(x_p = 2p\pi, y_p = 0)$, where p is an integer. Let us consider a dimer in the well centered on the minimum $(0, 0)$ and follow its behavior when its initial energy is increased. For a rigid dimer, $K > K_R = U_0/2$, the only other critical points of the potential energy surface are $[x_p = (2p + 1)\pi, y_p = 0]$, with p an integer, and they are saddle points with energy $4U_0$.

This dimer remains inside its energy well as long as its initial mechanical energy E_0 is smaller than $4U_0$. When $E_0 > 4U_0$, the system may get out of its well and drifts over the underlying potential with a center-of-mass motion $|x(t)| > \pi$ without large deformation that is for RC such that $|y(t)| < \pi$. When $K < K_R$, the points $[x_p = (2p + 1)\pi, y_p = 0]$ are local maxima and another set of saddle points exists. For $U_0/\pi < K < U_0/2$, these critical points are

$$x_p = (2p + 1)\pi, \quad \frac{2K}{U_0}y^* \\ = \sin y^* \quad E^* = 2U_0 \left(1 + \cos y^* + \frac{y^* \sin y^*}{2} \right) < 4U_0, \quad (9)$$

where p is an integer and E^* is the relevant energy. For these stiffnesses, an energy E^* is necessary to escape the potential well. Last, for a softer dimer, $K < K_S = U_0/\pi$, the set of points $[x_p = (2p + 1)\pi, y_p = 0]$ and $\{x_p = (2p + 1)\pi, y^* \in [\pi/2, \pi]\}$ both become local maxima, and there is another set of saddle points of smaller energy,

$$x_p = \pm \arccos \left(\frac{2K}{U_0} \frac{y_p}{\sin y_p} \right), \quad y_p = (2p + 1) \frac{\pi}{2}. \quad (10)$$

with p an integer. The energy of these saddle points with $p = 0$ is $E_S(K) = 2U_0 + K\pi^2/2 < U_0(2 + \pi/2) < 4U_0$. Such a soft dimer may escape its initial potential energy well for an even lower energy than in the previous cases.

This simple energetic analysis allows the identification of three regimes. When $(x(t), y(t))$ remains in their initial well, we will speak of a *trapped dimer* configuration. When the center-of-mass trajectory $x(t)$ evidences a monotonous time evolution, while the dimer undergoes small deformations with a RC such that $|y(t)| < \pi$, we will speak of a *sliding dimer* configuration. When the center of mass $x(t)$ extends on several wells with irregular and/or reversible hopping (hence $|x(t)| > \pi$) and/or when the dimer evidences a strong distortion with a RC such that $|y(t)| > \pi$, we will speak of a *jumping dimer* configuration.

These various configurations are illustrated in Figs. 2 and 3 which display the orthogonal projection of the dimer trajectory $(x(t), y(t))$ on the relevant potential energy surface (the actual dimer trajectory takes place in a constant mechanical

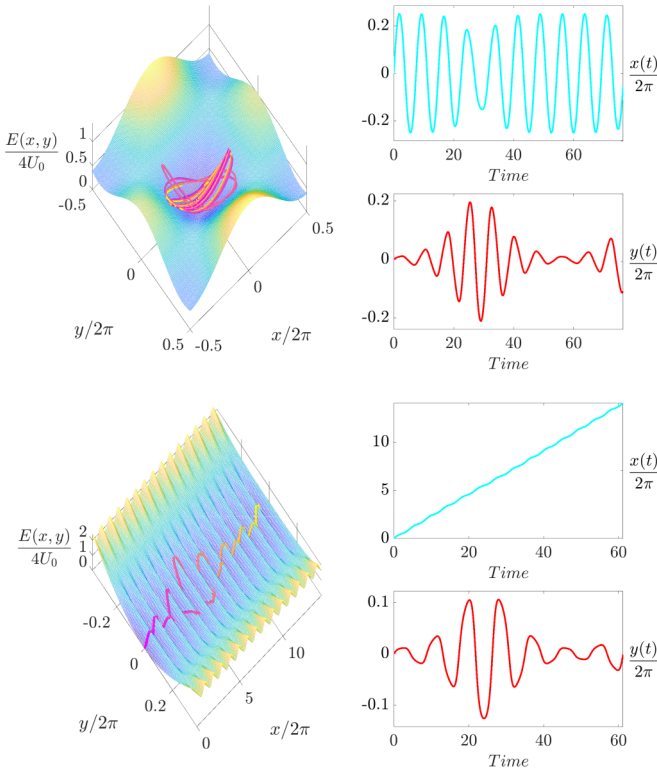


FIG. 2. Left panel: Potential energy surface (the energy increases from dark blue to yellow) with the orthogonal projection of the dimer trajectory on it (the time increases from pink to yellow). Right panel: Center-of-mass amplitude $x(t)$ (cyan) and RC amplitude $y(t)$ (red) as a function of time. Top plots: Trapped dimer, $E_0/4U_0 = 0.5$ and $K = 0.25K_S$. Bottom plots: Sliding dimer, $E_0/4U_0 = 1.2$ and $K = 1.75K_S$. See text for details.

energy plane). The top plots of Fig. 2 evidences an example of trapped dimer configuration. Its mechanical energy is both less than $4U_0$ and than $E_S(K)$. The center-of-mass and RC trajectories remain confined in the initial potential well. The bottom plots of Fig. 2 evidences a sliding dimer configuration for which the relevant mechanical energy is greater than $4U_0$. The center-of-mass trajectory is then a monotonous function of time that extends over several periods of the underlying periodic potential, whereas the RC trajectory exhibits a slow modulation with an amplitude that is much less than π .

In Fig. 3 we provide two examples of jumping configurations. In the top plots the dimer mechanical energy is less than $4U_0$ but greater than $E_S(K)$ and $K < U_0/\pi$. The dimer is thus energetically able to escape its initial potential energy well by the saddle point (10) as shown by the center-of-mass and RC trajectories. In the bottom plots, the dimer mechanical energy is greater than $4U_0$, and the center-of-mass motion is of much larger amplitude than the RC motion. In contrast with the bottom plots of Fig. 2, the center-of-mass trajectory is not a monotonous function of time.

B. Dynamical analysis

1. Perturbative approach

Beyond this energetic analysis, it is the opportunity of the parametric amplification of the RC by the center-of-mass

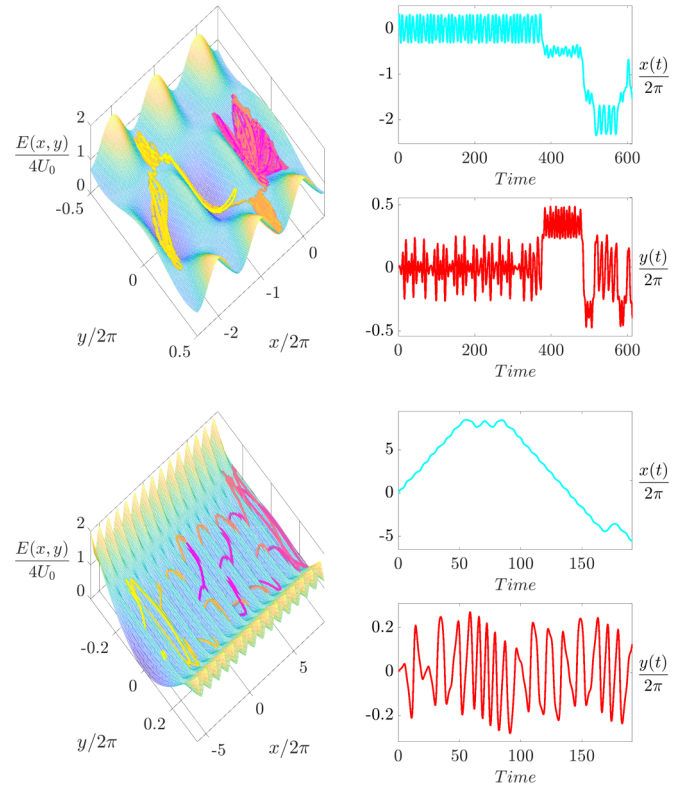


FIG. 3. Illustrations of the jumping regime. The color code is the same as in Fig. 2. Top plots: $E_0/4U_0 = 0.7$ and $K = 0.45K_S$. Bottom plots: $E_0/4U_0 = 1.05$ and $K = 1.2K_S$. See text for details.

motion as a consequence from their coupling which mainly determines the dynamics of x and y . Despite its apparent simplicity, the system of Eqs. (6) and (7) is not integrable and one must resort to approximations in order to find analytical expressions of x and y . In Ref. [15] we provide a rigorous analysis in two limiting cases. The key point was to exhibit a small parameter ϵ and to build a perturbation expansion in powers of ϵ that includes nonlinear effects in a consistent fashion.

For a trapped dimer, we set $\epsilon^2 = E_0/4U_0$ and we assume $|\epsilon| \ll 1$. Physically, this ensures that the dimer cannot escape the well in which it is initially set since in this case $E_0 < E_S(K)$. The center-of-mass amplitude x and the RC amplitude y are assumed to be of order $\mathcal{O}(\epsilon)$. Using a perturbation expansion, we obtain the amplitude equations for both motions, valid at order ϵ^3 . These amplitude equations evidence an *autoparametric instability* [12], that is, a parametric amplification of the RC motion by the center-of-mass motion, when the stiffness of the dimer interaction is of order $K = \mathcal{O}(\epsilon^2)$. A complete solution then may be found:

$$x(t) = 2\epsilon a \cos(\Omega_0 t + \phi), \quad y(t) = 2\epsilon b \cos(\Omega_0 t + \psi). \quad (11)$$

The frequency $\Omega_0 = \sqrt{U_0}$ is equal to one in our units. The relevant dynamical variables are the amplitudes a and b and the phase difference $\theta = 2(\phi - \psi)$ are found to be

slowly varying functions of time with dynamics given by the amplitude equations as

$$\frac{\partial a}{\partial s} = \frac{ab^2}{4} \sin \theta, \quad (12)$$

$$\frac{\partial b}{\partial s} = -\frac{a^2 b}{2} \sin \theta, \quad (13)$$

$$\frac{\partial \theta}{\partial s} = 2\tilde{K} + \frac{1}{2}(b^2 - a^2)(1 + \cos \theta), \quad (14)$$

where we set $K \equiv \epsilon^2 \tilde{K}$ with \tilde{K} of order one. The slow timescale s was found to be of order $\epsilon^2 t$. The autoparametric amplification of the RC by the center-of-mass motion happens for stiffnesses such that $0 < K \leq K_I(\epsilon)$, where $K_I(\epsilon) = \epsilon^2/2 = E_0/8U_0$.

The other limiting case studied in Ref. [15] is the sliding dimer, when the initial kinetic energy of the center of mass is such that the periodic potential is a small perturbation. In this configuration we assumed $|\epsilon^{-1}| \ll 1$. Physically, this is tantamount to assume that the dimer initial kinetic energy is much larger than the depth of the potential well. Then the dimer motion is basically a monotonous translation of the center of mass with small oscillations of particles around their equilibrium distance. Assuming $x = \mathcal{O}(1)$ and $y = \mathcal{O}(\epsilon^{-1})$ the amplitudes of the normal modes were found to be

$$x(t) = V_0 t + c \sin V_0 t, \quad y(t) = \frac{2}{\epsilon} b \cos(\sqrt{2K}t + \psi), \quad (15)$$

where $V_0 = \sqrt{E_0 - 2U_0}$ is simply the average center-of-mass velocity when it slides far above the periodic potential which then appears as an uniform potential of average value $2U_0$. In the sliding regime, $E_0 \gg U_0$, and thus $V_0 = \sqrt{E_0}(1 - U_0/E_0)$. E_0 is the kinetic energy given initially to the center of mass, so that the constant c is such that $E_0 = v_x(t=0)^2 = V_0^2(1 + c)^2$. Since c is a small correction, we get $c = U_0/E_0 = 1/4\epsilon^2$. The amplitude b and phase ψ are slowly varying functions that depends on the slow timescale $s = \epsilon^{-2}t$. A parametric resonance of the RC induced by the center-of-mass motion can happen if the dimer stiffness is strong enough. In our units the instability tongue is given by [16]

$$K_I^< \equiv \frac{E_0}{8U_0} - \frac{1}{2} \leq K \leq K_I^> \equiv \frac{E_0}{8U_0}. \quad (16)$$

2. Beyond the perturbative approach

The theoretical analysis of Ref. [15] is based on perturbation expansions that require a small parameter. By construction, its validity range is thus *a priori* restricted. In the trapped regime, we assume small stiffness and small motions, and in the sliding regime we assume monotonous center-of-mass motion, small RC, and a large stiffness. However, our previous numerical results suggest that the actual range of validity might be less restricted than expected. For instance, in the trapped regime, the phase portrait of the amplitude equations (12), (13), and (14) evidences an excellent agreement with the numerical simulations for $\epsilon \approx 0.224$ (that is, $E_0/4U_0 \approx 0.050$). In the sliding regime, an excellent agreement between the simulations and the predictions of the amplitude equation is observed for $\epsilon^{-1} = 0.35$ (that is,

$E_0/4U_0 \approx 8.16$), and we have to take $\epsilon^{-1} = 0.63$ ($E_0/4U_0 \approx 2.52$) to observe significant discrepancies.

The simulations of Ref. [15] were designed to test the validity of our theoretical analysis, and consistently they were limited to small values of the relevant perturbative parameter. A necessary condition for the validity of the perturbation expansions, whether in the case of a trapped dimer or in the case of a sliding dimer, is the smallness of the RC amplitude. One of the purposes of the present work is to extend the parameter range outside the requirements of the perturbation expansions. Large values of the relevant perturbative parameter are needed to evidence significant quantitative discrepancies, and most qualitative features are observed up to the largest available values. For instance, in the trapped regime, the frontier between parametrically stable and unstable systems extends on the whole range $0 \leq E_0/4U_0 \leq 1$. Moreover, we identify in what follows the parameter ranges in which the jumping takes place.

III. OVERVIEW OF DIMER MOTION

In this section, we summarize the dimer motion observed in our simulations in the relevant parameter space $\{K, E_0/4U_0\}$. We numerically integrate the system (6) and (7) using the Verlet algorithm [17], with a time step of 7.7×10^{-3} in dimensionless units. We explore the range $0 \leq K \leq 0.633$ on the abscissa and $0 \leq E_0/4U_0 \leq 2$ on the ordinate. The resolution on the abscissa axis is 1.40×10^{-5} for $E_0 \leq 4U_0$ and 1.60×10^{-5} for $E_0 \geq 4U_0$. The resolution on the ordinate axis is 2.00×10^{-3} . The whole results are provided by 535 000 numerical simulations, of duration $\Delta t = 3.07 \times 10^3$ in dimensionless time. The analysis of such an amount of simulations requires some automatic analysis process, in particular to identify the parametric instability threshold. This process is discussed in Sec. III A. The behavior map is displayed and discussed in Sec. III B.

A. Identification of the parametric instability

The main characteristic of the parametric resonance of the RC is the exponential growth of its amplitude, which is not easy to detect since it is only a transient. To overcome this difficulty, we have performed a numerically efficient process that provides a clear evidence when the dimer gets inside its domain of instability. Indeed, when the initial phase difference between the center-of-mass and RC motions is well chosen, the initial behavior of the RC motion is radically different on both sides of the instability boundary.

Our automatic process consists in ascertaining the initial variation of the RC amplitude $y(t)$ as a function of time. Let us first consider the trapped case. In our simulations process, we seek the possibility of parametric instability of the RC then the initial energy E_0 is almost entirely given to the center of mass. In order to apply the same method in all simulations even for the sliding case, this initial energy is injected as the kinetic energy of the center of mass. A very small perturbation of the RC triggers the instability (the relevant energy is $10^{-3}E_0$).

In the trapped configuration the initial phase difference $\theta(t=0) \equiv \theta_0$ indicates whether this disturbance is kinetic ($\theta_0 = 0$) or elastic ($\theta_0 = \pi$). If this perturbation is such that

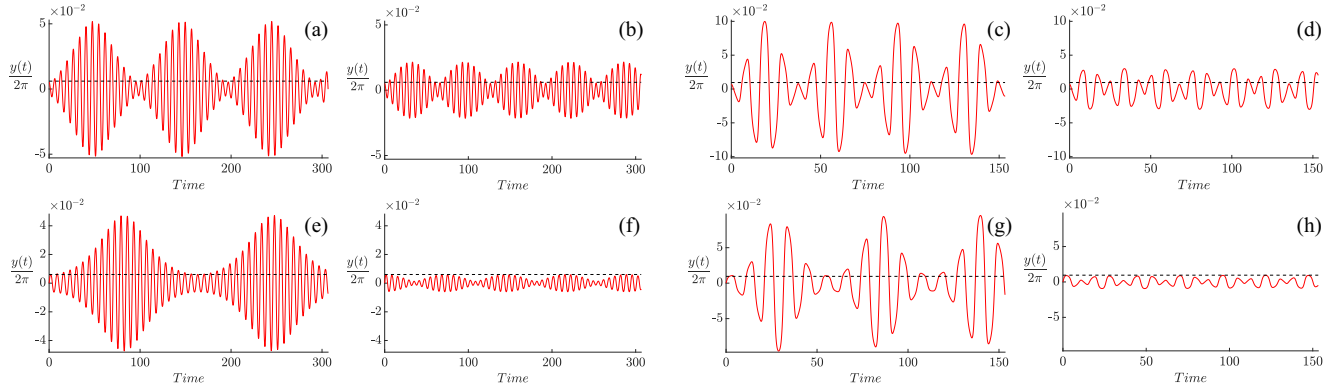


FIG. 4. RC amplitudes $y(t)$ as a function of time for an initial phase $\theta_0 = \pi$ [(a)–(d)] and $\theta_0 = 0$ [(e)–(h)]. For plots (a) and (b) and then (e) and (f) we set $\epsilon = \sqrt{E_0/4U_0} = 0.60$ and for plots (c) and (d) and then (g) and (h) we set $\epsilon = 0.95$. In plots (a), (c), (e), and (g) the stiffnesses are such that $K = K_I(\epsilon) - \delta K(\epsilon)$ with $\delta K(\epsilon) = K_I(\epsilon)/20$, and consistently $y(t)$ evidences a parametrically unstable behavior. In plots (b), (d), (f), and (h) the stiffnesses are such that $K = K_I(\epsilon) + \delta K(\epsilon)$, and consistently $y(t)$ evidences a stable behavior. The black dashed lines indicate the square root of the initial energy of the RC.

$\theta_0 = 0$, then we observe that the RC amplitude $y(t)$ initially increases when the system is in the parametric instability domain whereas it decreases when the system is parametrically stable. In contrast, if the disturbance energy is a potential elastic energy ($\theta_0 = \pi$), then the RC $y(t)$ increases on both side of the transition border. This is consistent with our model for small values of ϵ . Indeed, with initial conditions $a_0 \neq 0$, $b_0 \ll a_0$, and θ_0 , a linear stability analysis of Eqs. (12) to (14) provides the initial evolution of $b(t)$. If $\theta_0 = 0$, then we get $\delta\dot{\theta} \simeq 2\tilde{K} - 1$. Therefore, b will begin to decrease if $\tilde{K} > 1/2$ and then $\sin \theta > 0$ and to increase if $\tilde{K} < 1/2$ so that $\sin \theta < 0$. In contrast, for $\theta_0 = \pi$ we get $\delta\dot{\theta} = 2\tilde{K} \geq 0$, so θ and $b(t)$ will begins to increase, with $\sin \theta < 0$, regardless of the value of the stiffness.

These changes of behavior along the instability boundary are consistent with the perturbative analysis. Indeed, at the instability boundary $\tilde{K} = 1/2$, there is a fixed point $a = 1$, $b = 0$, and $\theta_0 = 0$ of the amplitude equations. However, this effect is not restricted to small values of $E_0/4U_0$ and takes place for values of ϵ that are far away from the perturbative method requirements. This is evidenced in Fig. 4, which displays clear changes of initial evolution of y when $\theta_0 = 0$ and when $\theta_0 = \pi$ for the rather large value $\epsilon = 0.95$. Therefore, we use this method to automatically identify the parametric instability boundaries in the whole range $0 \leq \epsilon \leq 1$.

In the sliding configuration the initial phase $\psi(t = 0) \equiv \psi_0$ indicates whether the initial disturbance is provided by kinetic energy ($\psi_0 = \pi/2$) or potential elastic energy ($\psi_0 = 0$). In this configuration, two parametric instability boundaries have to be identified. In order to use the same kind of automatic determination of the boundaries, the most appropriate initial phase ψ_0 has to be chosen for each of them. As in the previous case, we use our previous perturbative analysis out of its validity range. The assignment procedure is detailed in Appendix C.

B. Behavior map

The dimer motion observed in our simulations are summarized in the behavior map shown in Fig. 5, which indicates the state of the dimer as a function of the control parameters. At

first glance, we can assign domains in the plane $\{E_0/4U_0, K\}$ to the three kinds of configurations (trapped, sliding, jumping) described in Sec. II A.

Below the transition line $K_I(\epsilon)$ (orange line in Fig. 5), the dark blue area corresponds to parametrically stable RC oscillations. Above this line, we find an area where the RC oscillations are parametrically unstable (light blue). This is consistent with the perturbative analysis of Sec. II B 1 about the autoparametric instability of the dimer, but it is quite remarkable that the threshold $K_I(\epsilon)$ extends to the whole range of ϵ , even when the perturbation expansion requirements are not *a priori* fulfilled.

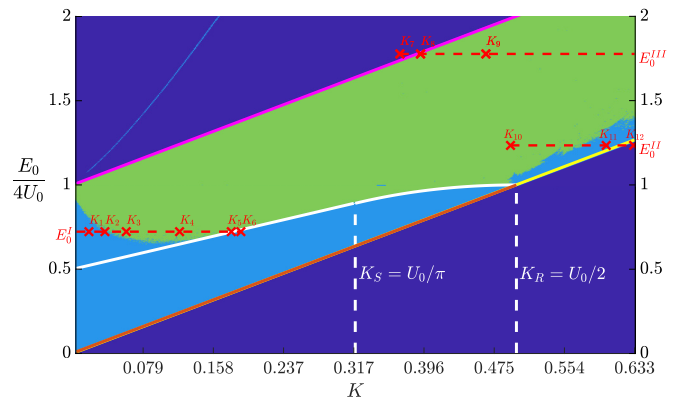


FIG. 5. Map of dimer behavior. This map is established for an initial energy of the RC $0.001E_0$, the initial phase difference is $\theta_0 = 0$ (i.e., $\psi_0 = \pi/2$ in the case $E_0 \leq 4U_0$ and $\psi_0 = 0$ in the case $E_0 \geq 4U_0$). The dark blue areas represent a parametrically stable RC. The light blue areas represent a parametrically unstable RC. The green area represents a jumping motion of the system. The orange line is the instability threshold K_I , the yellow line is the instability threshold $K_I^<$, and the magenta line the instability threshold $K_I^>$. The white curve represents the minimal necessary energy for a given stiffness to observe a jumping motion. The white vertical dashed lines indicate the stiffnesses K_S and K_R . The center-of-mass and RC motions are plotted in Fig. 13 for energy E_0^I , in Fig. 15 for energy E_0^{II} , and in Fig. 14 for energy E_0^{III} .

For $E_0 < 4U_0$ ($\epsilon^2 < 1$), let us describe the dimer motion when we increase the initial energy of the dimer at a given stiffness $K < U_0/2$. At low initial energy the dimer motion is stable, then as the initial energy increases the RC motion becomes parametrically unstable and eventually at larger initial energy the dimer motion reaches the jumping regime (the green area). The straight white line $\epsilon^2 = 1/2 + K\pi^2/8U_0$, which corresponds to the energy of the saddle point of Eq. (10) for $0 \leq K \leq U_0/\pi$, and the white curve $E^*(y^*)$, which is an implicit function of K and corresponds to the energy of the saddle point of Eq. (9) for $U_0/\pi \leq K \leq U_0/2$, have been plotted. As shown in Sec. II A, an initial energy above these limits allows large motion of the dimer. For $K > 0.1$, the agreement between the predictions of our energetic analysis is excellent because the jumping regime consistently happens above these theoretical limiting curves. However, at smaller stiffness, there is a surprising domain with $K < U_0/\pi$ and $\epsilon^2 > 1/2 + K\pi^2/8U_0$ in which the dimer is not in the jumping regime as expected but remains trapped. This is not an artifact of our automatic analysis of the simulations data. To verify this point, we show in Fig. 13 the dimer trajectories registered for the constant initial energy E_0^I and for stiffnesses that increases from K_1 to K_6 . This figure is discussed further in Sec. VI, but we already remark that it confirms the identification of the various areas in the behavior map.

When $E_0 > 4U_0$ ($\epsilon^2 > 1$), the dimer motion may exhibit stable sliding, with one-way translation of the center of mass and small oscillations of the RC, parametrically unstable sliding with large oscillations of the RC and an oscillatory motion of the center of mass overlaid on its one-way translation, or a jumping behavior with nonmonotonous translation of the center of mass and large oscillations of the RC. We have plotted on the map the transition lines of the parametric instability $K_I^<$ and $K_I^>$ deduced from the perturbative analysis. The behavior map in Fig. 5 is restricted to rather small values $1 \leq E_0/4U_0 \leq 2$, so that the relevance of the perturbation expansion is questionable. Along the border $K_I^<$, for a given energy E_0 , the dimer behavior changes from a stable amplitude oscillation to a jumping regime when K increases. This is confirmed by the direct observation of the dimer trajectories, as shown in Fig. 14, where we plot the dimer trajectories registered for the constant initial energy E_0^{II} and for stiffnesses that increases from $K_7 < K_8 < K_9$. The upper trajectories for $K = K_7$ [slightly lower than $K_I^<(E_0^{III})$] clearly display a parametrically stable motion, whereas the middle trajectories for a stiffness $K = K_8$ [slightly greater than $K_I^<(E_0^{III})$] clearly displays a jumping motion.

The border $K_I^>$, at these small values of the parameter $E_0/4U_0$, is rather irrelevant to describe the parametric instability of the RC. This is shown in Fig. 15, where we plot the dimer trajectories registered for the constant initial energy E_0^{II} and for stiffnesses $K_{10} < K_{11} < K_{12}$. There is no difference in the trajectories for K_{11} and K_{12} which are on opposite sides of the transition line $K_I^>(E_0^{III})$.

In the stable domain $K < K_I^<$, a very thin domain with unstable RC motion is seen (thin cyan line in the upper left corner of Fig. 5). In this domain, the RC motion evidence characteristics that are similar to a parametric resonance. We interpret this behavior as a nonlinear effect that induces a parametric amplification of the RC motion when its frequency ($\sqrt{2K}$) is equal to $V_0/4$. Such an effect has been described in

Refs. [18,19], and we discuss the link between these papers and our system in Appendix B. In the Supplemental Material of this paper [20] we display some RC trajectories and their Fourier transform which evidence such a parametric amplification. The most convincing evidence is that the frequency of the RC motion is found to be $V_0/4$, in agreement with the theoretical analysis [18,19]. Let us add that the identification of such a thin domain in the map of Fig. 5 confirms the practical efficiency of the automatic process used to identify the resonances.

IV. TRAPPED REGIME

Let us describe now in more detail the trajectories observed in the trapped regime. In each simulation described in this section the center-of-mass motion and the RC are oscillatory, with an amplitude that is smaller than a period of the external potential.

In Fig. 6 we give examples of the RC motion, $y(t)$, when we follow the transition line for the parametric instability, $K_I(\epsilon)$. We consider three values of ϵ , namely $\epsilon = 0.1$ which is consistent with the perturbative analysis, and $\epsilon = 0.4$ and $\epsilon = 0.7$, which are significantly larger. In the upper panel the stiffness is far away from the transition line, and we observe a small RC amplitude, with a smaller slow modulation. We are very far from the autoparametric amplification limit, so that the energy exchange between the center-of-mass motion and the RC are inefficient. In the center panel, the stiffness is much closer to the transition line but still above. The RC amplitude is still small, numerically very close to its value in the upper panel, but two features foreshadow the parametric resonance. The modulation of the RC amplitude is proportionately higher, and the modulation timescale is much slower than in the previous case. These beats result from the approximate tuning of the frequencies of the center of mass and RC [21]. In the bottom panel, the stiffness is below the parametric instability transition line. Whatever the initial energy injected in the system, the simulation data evidence the autoparametric amplification of the RC. When compared to the previous cases, the RC amplitude is found to be an order of magnitude larger, the modulation is of much higher relative amplitude, and the characteristic modulation timescale is much slower. Moreover, the modulation of the RC amplitude is clearly not sinusoidal. The RC exhibits a slow periodic modulation, which physically traces back to the periodic transfer of energy between the center-of-mass motion and the RC. This periodic energy transfer is characteristic of autoparametric amplification in a conservative system [12,14,15].

We focus on this energy transfer in Fig. 7, where we plot the center-of-mass motion $x(t)$ (top, left plot), the RC $y(t)$ (top, right plot), and the parametric resonance tongue (bottom). The duration of the plots is limited to one period of slow modulation. We have verified the energy conservation in the simulations, and consequently a decrease of the center-of-mass motion amplitude $x(t)$ is observed when the RC amplitude $y(t)$ increases. Taking advantage of these very slow modulation timescales (note that the fast oscillations are not resolved), we can define instantaneous frequencies Ω_x and Ω_y for the dimer fast oscillations. The RC amplitude is parametrically amplified by more than 50, but it remains

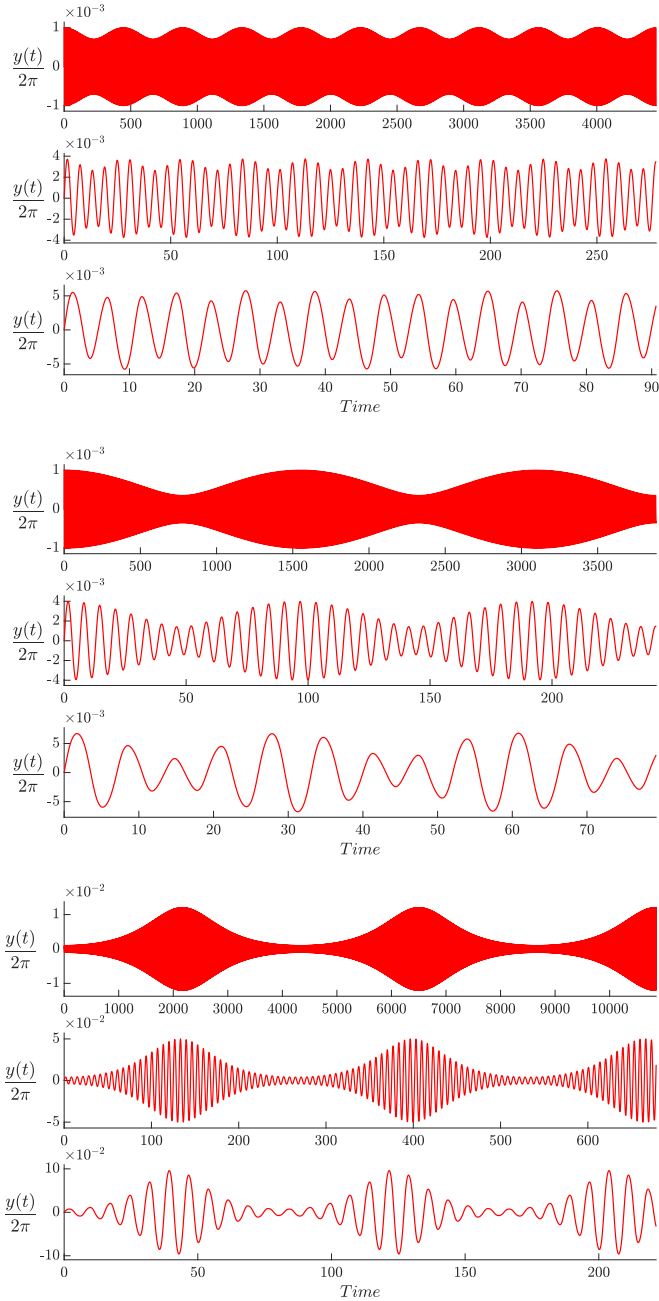


FIG. 6. RC amplitude $y(t)$ as a function of time (pay attention to the abscissae scale) in the parametrically stable cases (upper and center panels) and parametrically unstable case (lower panel). From top to bottom for each panel: $\epsilon = 0.10$, $\epsilon = 0.40$, and $\epsilon = 0.70$. Upper panel: $K = 1.00 \epsilon^2$; middle panel: $K = 0.57 \epsilon^2$; lower panel: $K = 0.43 \epsilon^2$. The dimer is parametrically unstable for $K_I \leq \epsilon^2/2$.

much less than the external potential period. Therefore, the RC may be described in first approximation by an effective Mathieu equation (see Appendix A), which allows us to describe the stability chart for parametric amplification in the plane $(\Omega_y/\Omega_x, h)$, as seen in the bottom plot of Fig. 7. The points numbered from 1 to 6 are indicated on the center-of-mass motion plot, and they are shown in the stability chart for their relevant fast oscillation frequency ratio Ω_y/Ω_x and their corresponding forcing amplitude h . As can be seen, the

parametric amplification stops when the parameters Ω_y/Ω_x and h reach the parametric instability boundary. The direction of energy transfer is then reversed until the system returns to its initial position, and so on. It appears that when the system is within the parametric instability tongue, even if the relevant parameters change on a slow timescale, the autoparametric resonance ensures that this conservative system cannot exit the instability tongue.

In order to verify the relevance of the parametric forcing of the RC by the center-of-mass motion, we plot in Fig. 8 the evolution of the Fourier spectra of $x(t)$ and $y(t)$ for $\epsilon = 0.4$ when the stiffness $K(\epsilon)$ decreases from a value far above the transition line $K_I(\epsilon)$ (the top four plots in Fig. 8) toward a value that is just below this transition line, so that the system is parametrically unstable (the bottom plot of Fig. 8). The center-of-mass motion does not depend on the stiffness, and consistently the relevant peak Ω_x in the Fourier spectrum (cyan solid curve) is basically the same in all plots. The frequency spectrum for the RC (red solid curve) exhibits a peak at a higher frequency Ω_y than for the center-of-mass motion, which consistently decreases with the stiffness. In the intermediate stiffness range (plots 2 to 4 from top to bottom) the slow modulation of the RC by the center-of-mass motion is reflected in the emergence of a low frequency peak due to the nonlinearities, roughly $\Omega_y - 2\Omega_x$ (note that another peak at $\Omega_y + 2\Omega_x$ may be seen if we extend the abscissa axis). Eventually, when the parametric instability threshold is reached, these three peaks merge in a large peak with several harmonics. When the system is parametrically unstable, the fast oscillations frequencies of the oscillators x and y are perfectly tuned and both spectrum display a single peak enriched by harmonics. This frequencies merging evidences the parametric instability.

The numerical data so far show that the transition line $K_I(\epsilon)$, which is calculated perturbatively for small ϵ , has a much larger validity range, up to $\epsilon \rightarrow 1$. In order to strengthen this observation, we compare the simulations data to other predictions deduced from the perturbative analysis. In practice, we compare the amplitude extrema of the motions $x(t)$ and $y(t)$ and their slow modulation period T given by our perturbative analysis to our numerical simulations.

As seen in Fig. 7 the center-of-mass and the RC amplitudes exhibit a minimum x_{\min} and a maximum y_{\max} , respectively. These extrema are derived in Ref. [15] and when recast in our units they read

$$x_{\min}^2 = 8K, \quad y_{\max}^2 = E_0 - 8K. \quad (17)$$

These expressions are derived for a parametrically unstable system. In the parametrically stable domain ($K > \epsilon^2/2$) there is basically no energy transfer between the two oscillations modes and the oscillation amplitudes do not depend on K . In contrast, in the parametrically unstable domain, both extrema strongly depend on K . In the left panel of Fig. 9 we plot the amplitude extrema deduced from the simulations data as a function of K (symbols) and compare them to Eq. (17) (solid line), for several values of ϵ . This agreement is excellent for $\epsilon \leq 0.4$ and it requires a large value, $\epsilon = 0.7$, to evidence a clear discrepancy.

An analytic expression of the slow modulation period for a parametrically unstable system is easily found from

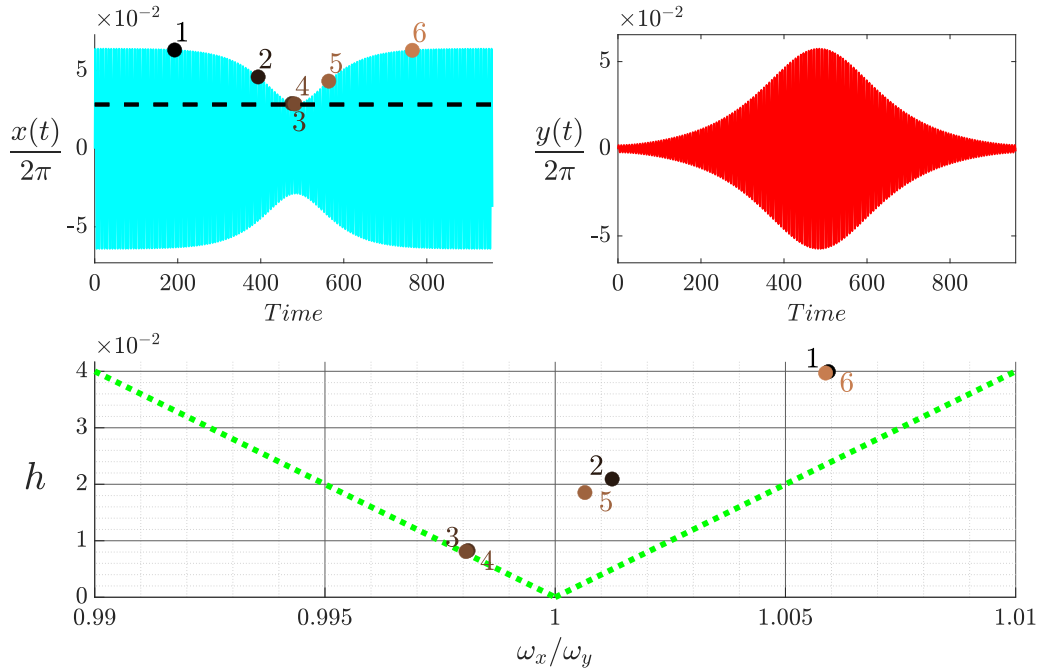


FIG. 7. Upper panel: Amplitudes of the center-of-mass motion (cyan) and RC (red) as a function of time for $\epsilon = 0.2$ and $K = K_I(\epsilon)/5$. The black dashed line indicates the minimum amplitude of the center-of-mass motion, Eq. (17). Lower plot: Instantaneous positions of the system in the parametric instability tongue (green dotted lines). See Appendix A.

Eqs. (25) to (27) of Ref. [15]. In the right panel of Fig. 9 we compare the analytical expression of T (solid line) to the numerical estimate (symbols) as a function of K for several values of ϵ . This period may be also easily deduced from the simulation data, since it is the time interval between two amplitude extrema. In the parametrically stable domain, T is the period of the beats between the center-of-mass motion

and the RC, and its growth is due to the frequencies merging discussed before. Another way to interpret the divergency of the period T is by the critical slowing down at the parametric instability threshold. The agreement between the simulations data and the analytic predictions is excellent for $\epsilon \leq 0.4$ and it requires a large value, $\epsilon = 0.7$, to evidence a clear discrepancy.

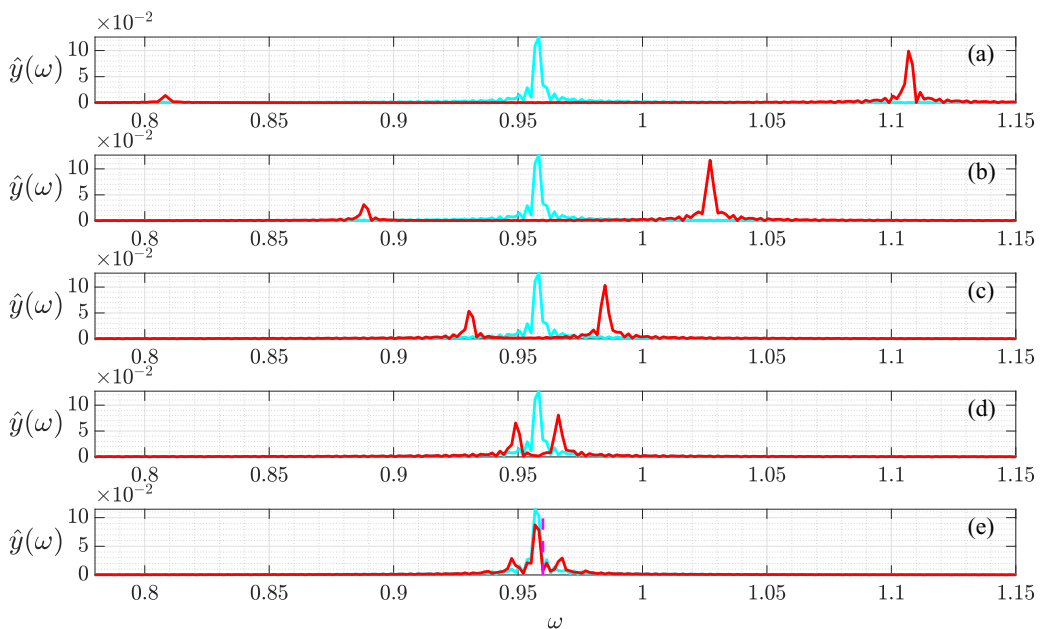


FIG. 8. Fourier transforms of the center-of-mass (cyan) and RC (red) amplitudes for $\epsilon = 0.4$. The stiffness K is (a) $2.5K_I(\epsilon)$, (b) $1.5K_I(\epsilon)$, (c) $1.1K_I(\epsilon)$, (d) $1.01K_I(\epsilon)$, and (e) $0.99K_I(\epsilon)$. The plot (e) corresponds to a parametrically unstable dimer, the plots (a)–(d) to a stable dimer.

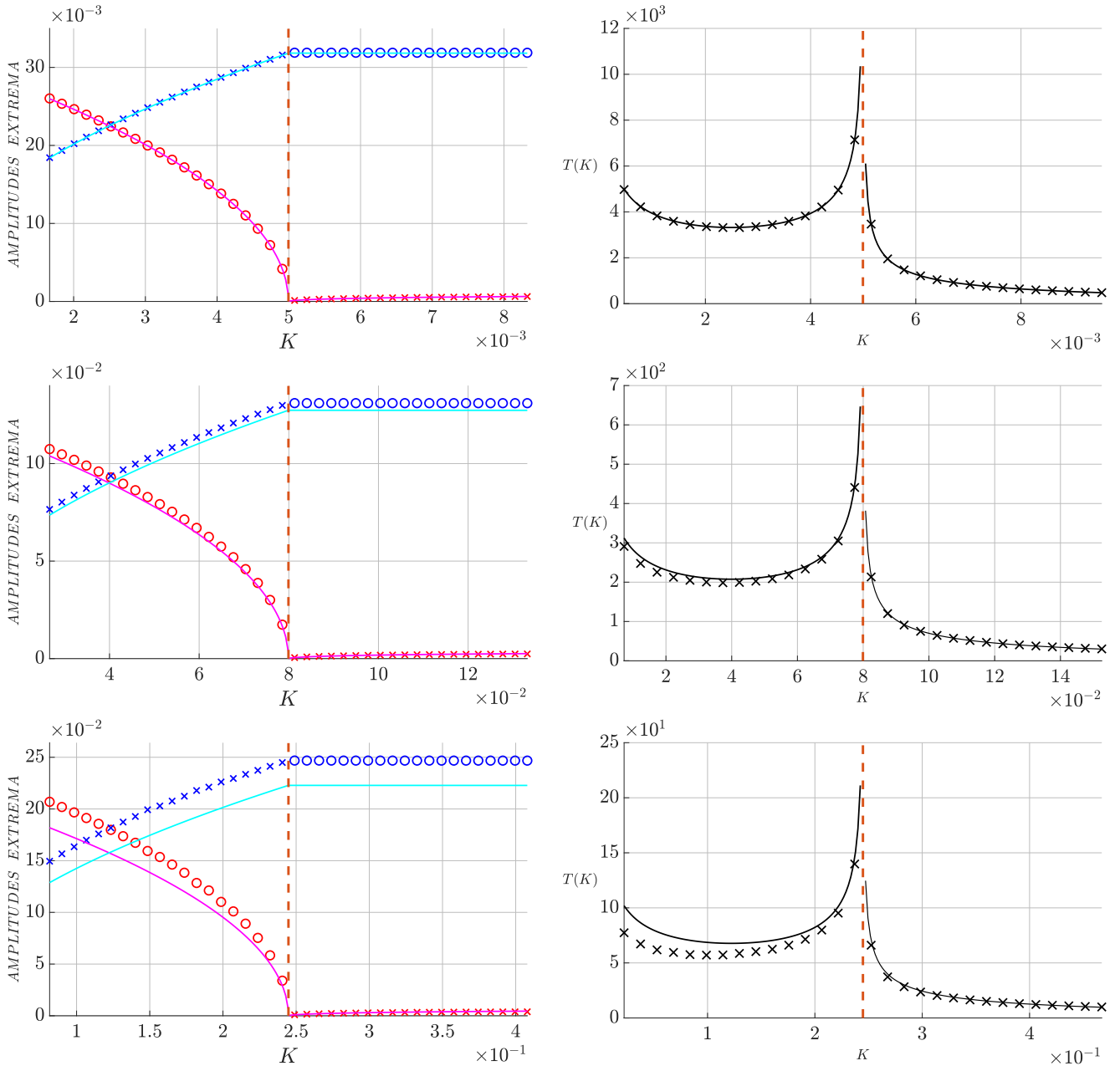


FIG. 9. Extrema (left panel) of center-of-mass (blue and cyan) and RC (red and magenta) amplitudes and periods (right panel) of their energy transfer as a function of the stiffness K . From top to bottom: $\epsilon = 0.1$; 0.4 ; 0.7 . The solids lines are analytical predictions, the dots simulations data. Left panel: Maxima (open circles) and minima (crosses) of the amplitudes. In all plots the orange dashed line represent the frontiers of instability for the relevant ϵ [i.e., $K_I(\epsilon)$]. Left side of the orange dashed line: RC is parametrically unstable. Right side of the orange dashed line: RC is stable.

The center-of-mass and the RC amplitudes, together with their characteristic modulation times both confirm that our perturbative method is a good guide to analyze the features of the trapped regime on a much wider range of ϵ than what may be expected *a priori*.

V. SLIDING REGIME

This regime is reachable when $E_0 > 4U_0$, and the relevant perturbative analysis assumes that ϵ^{-1} is a small parameter (see Sec. II B 1). The center-of-mass trajectory is basically a

translation, but the underlying periodic potential induces some oscillations around a straight trajectory. These oscillations are the weaker the higher the kinetic energy of the center of mass. As an example, we show in Fig. 10 two center-of-mass trajectories. A quantitative comparison between the simulations data and the theoretical analysis, Eq. (15), evidences an excellent agreement for $\epsilon^{-1} = 0.40$, which is to say that the validity range of the perturbative analysis is roughly $0 < \epsilon^{-1} \leq 0.4$. Some discrepancies are seen for $\epsilon^{-1} = 0.95$, but even for this very high value of the perturbation parameter the qualitative features of the sliding regime are very well described.

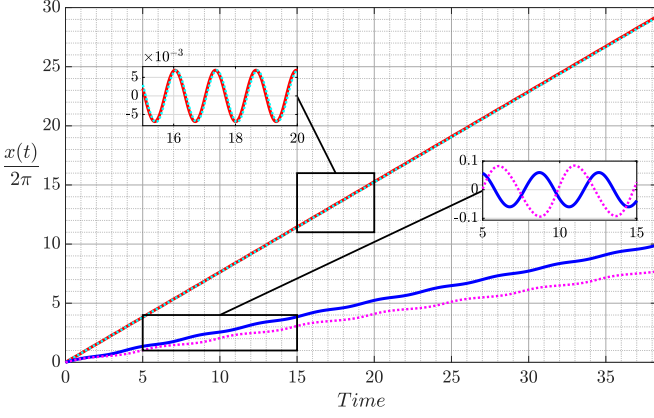


FIG. 10. Trajectories of the center of mass in the sliding regime for $K = 3K_R/2$. The dotted lines represent the numerical simulations. The solid lines are the analytic results of Eq. (15). Red and cyan curves: $\epsilon^{-1} = 0.4$; blue and magenta curves: $\epsilon^{-1} = 0.95$. Insets: We highlight the modulation of the center-of-mass trajectory by subtracting a linear fit for the numerical simulation (dashed line) and compare it to the oscillating component of the center-of-mass motion given by Eq. (15) (solid line).

In the sliding regime, from the results of the perturbative analysis, we expect for the RC a parametric instability, for a given parameter ϵ^{-1} , when the stiffnesses K is such that $K_I^<(\epsilon^{-1}) \leq K \leq K_I^>(\epsilon^{-1})$. In Fig. 11 we display the RC amplitude as a function of time very near the two instability threshold $K_I^<$ and $K_I^>$ for an initial energy such that $\epsilon^{-1} = 0.4$. In the parametrically unstable domain, the parametric amplification is exhibited by the simulation data with an amplification ratio that is almost 200 for $K > K_I^<(\epsilon^{-1})$ and 200 for $K < K_I^>(\epsilon^{-1})$, and the characteristic timescale for this amplification is very slow. In the parametrically stable domain, since we are close to the threshold, the characteristic slow timescale beats are observed. In our conservative autoparametric system, the RC in the parametrically unstable domain is periodic, but the plots in Fig. 11 are limited to a single period.

The autoparametric instability may also be illustrated in the frequency domain. In the sliding regime, the basic motion of the center of mass is a translation with average velocity V_0 , as seen from Eq. (15). Assuming a small amplitude of the RC motion, and injecting the basic center-of-mass motion in Eq. (7), we get for y a Mathieu equation with a forcing induced by the center-of-mass motion at frequency V_0 , and hence a parametric instability at frequency $V_0/2$. For a parametrically stable dimer, the characteristic frequency of the RC is $\sqrt{2K}$. We plot in Fig. 12 the frequency spectrum of the RC when $K \rightarrow K_I^<$ (top panel) and $K \rightarrow K_I^>$ (top panel). In both panels the stiffness increases from top to bottom. When $K < K_I^<$ the RC exhibits a frequency peak below the forcing frequency $V_0/2$. When K increases, this peak moves to the left and another peak appears above $V_0/2$. This latter is due to the nonlinearities. Eventually, when $K \rightarrow K_I^<$ the parametric instability is reached and the RC motion synchronizes with the parametric forcing frequency (see bottom plot of top panel). In this case, because of the parametric amplification the RC motion becomes an oscillation with a large amplitude modulation

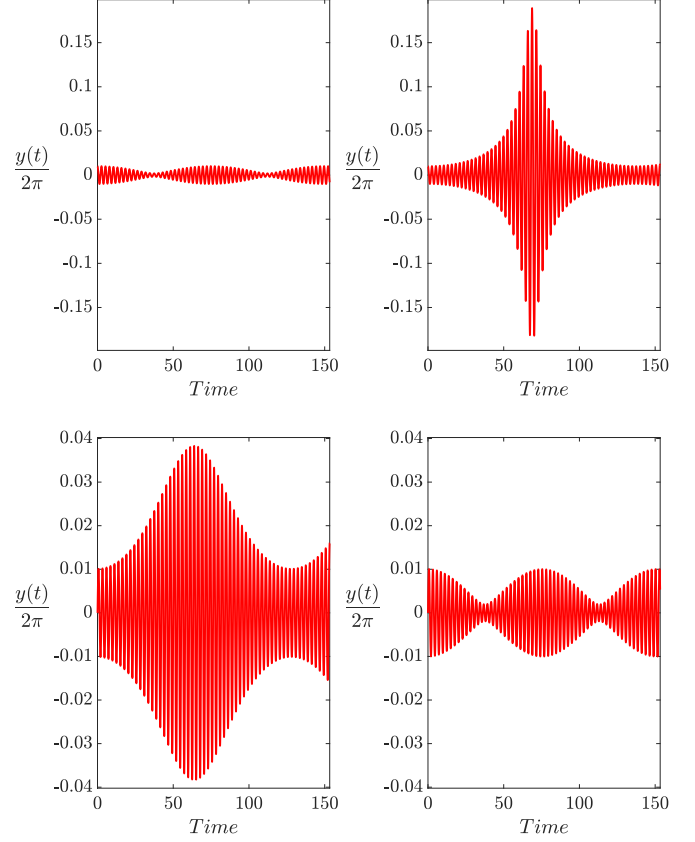


FIG. 11. Trajectories of the RC for $\epsilon^{-1} = 0.4$ very close to the thresholds of parametric instability $K_I^<(\epsilon^{-1})$ and $K_I^>(\epsilon^{-1})$. Upper panel: $\psi_0 = 0$; left plot: $K = 0.993K_I^<(\epsilon^{-1})$ (stable); right plot: $K = 1.007K_I^<(\epsilon^{-1})$ (unstable). Lower panel: $\psi_0 = \pi/2$; left plot: $K = 0.993K_I^>(\epsilon^{-1})$ (unstable); right plot: $K = 1.007K_I^>(\epsilon^{-1})$ (stable).

(see the upper right plot in Fig. 11) and consistently its frequency spectrum evidences many harmonics. When $K > K_I^>$ the RC exhibits a frequency peak above the forcing frequency $V_0/2$. Reading the lower panel from bottom to top, we get the same features as in the previous case. In the parametrically unstable case (top plot of lower panel in Fig. 12) the frequency spectrum is rather poor in harmonics, which is consistent with the rather small parametric amplification of the RC in that case (see the lower left plot in Fig. 11).

VI. JUMPING REGIME

Let us now consider the jumping regime, which means that basically motion of the center of mass is neither oscillating nor monotonic, and the particles are no more separated by a single potential period.

For $E_0/4U_0 < 1$, a necessary condition to observe the jumping regime is $E_0 > E_S(K)$, where the energy of the saddle point is $E_S(K) = 2U_0 + K\pi^2/2$ for $K < K_S$ and $E_S(K) = E^*$ defined in Eq. (9) for $K_S < K < K_I$ as discussed in Sec. II A. When this condition is met, the dimer center of mass may get out of its initial potential well and/or the RC amplitude may extend on more than a single period of the external potential. However, this condition is not sufficient as seen in Sec. III B since there is a domain in Fig. 5 with $E_0 > E_S(K)$

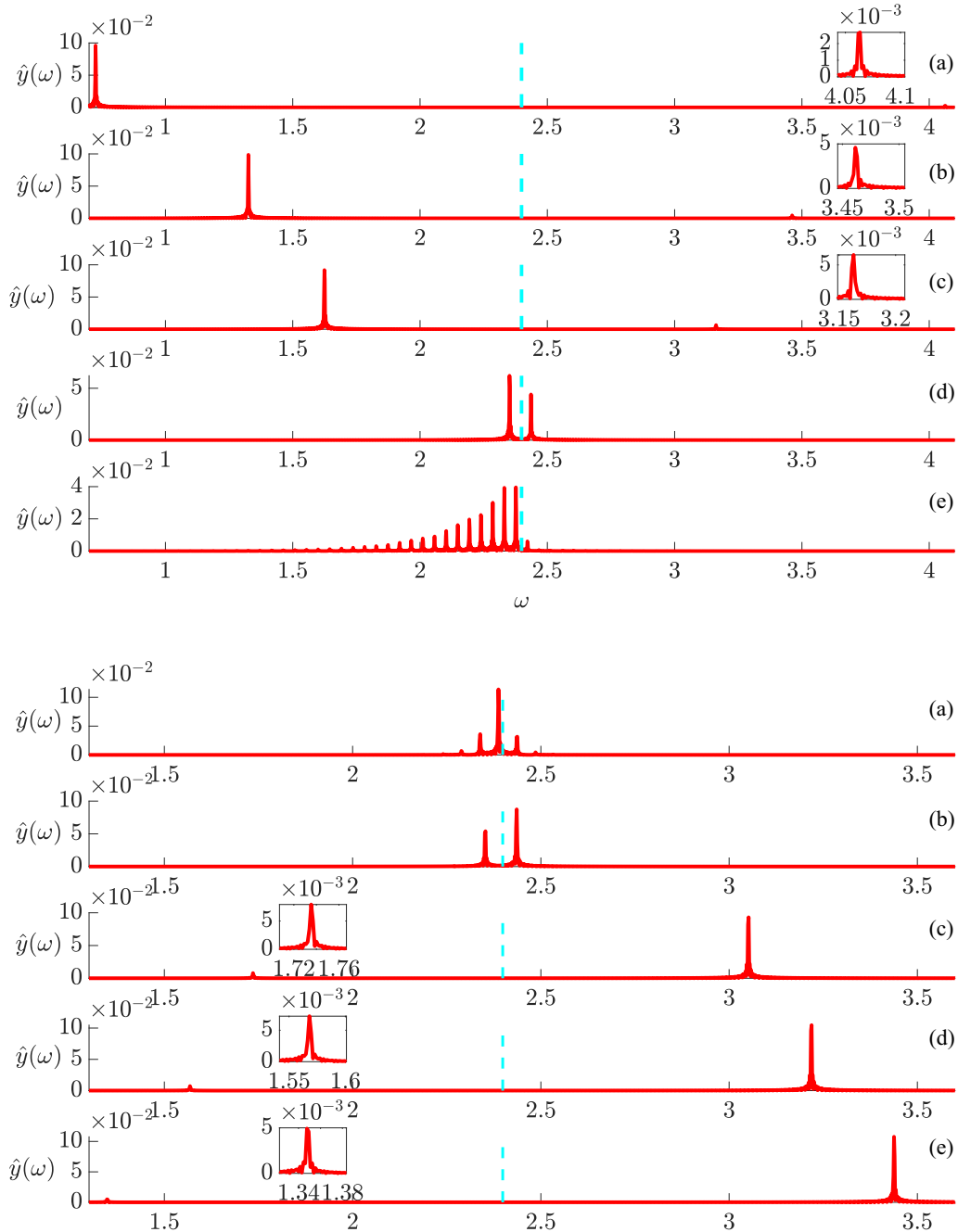


FIG. 12. Fourier transforms of the relative motion at $\epsilon^{-1} = 0.4$. Upper panel: $\psi_0 = 0$. From top to bottom: $K = 0.100 K_I^<(\epsilon^{-1})$, $0.333 K_I^<(\epsilon^{-1})$, $0.500 K_I^<(\epsilon^{-1})$, $0.993 K_I^<(\epsilon^{-1})$, and $1.007 K_I^<(\epsilon^{-1})$. Lower panel: $\psi_0 = \pi/2$. From top to bottom: $K = 0.993 K_I^>(\epsilon^{-1})$, $1.007 K_I^>(\epsilon^{-1})$, $1.500 K_I^>(\epsilon^{-1})$, $1.667 K_I^>(\epsilon^{-1})$, and $1.900 K_I^>(\epsilon^{-1})$. Cyan dashed line: $V_0/2$. The insets are zooms on peaks of small amplitude.

and a small stiffness (roughly $K < 0.1$) in which the system evidences trapped motion. In order to clarify this observation, we have selected several dimers with increasing stiffnesses from K_1 up to K_6 , with the same initial energy E_0^I . Following our automatic detection process (see Appendix C), the dimers with K_1 and K_2 are in a trapped regime, the dimers with K_3 , K_4 , and K_5 are in a jumping regime, and, last, the dimer with K_6 is in a trapped regime, as indicated in Fig. 5. This is indeed confirmed by the plots of the center-of-mass motion $x(t)/2\pi$ and of the RC $y(t)/2\pi$ displayed in Fig. 13. Note

that in the trapped regimes the dimer is always parametrically unstable, which explains the large modulation of both amplitudes.

The configurations $K \in [K_1, K_6]$ correspond to a parametrically unstable RC because $E_S(K)$ is always greater than the instability limit. The initial evolution of y are thus always exponential but only the dimer for which the amplitude of y reaches a critical value, roughly equal to $\pi/2$ may escape suggesting that the dimer escapes through the vicinity of the saddle points and not strictly through these points. This is

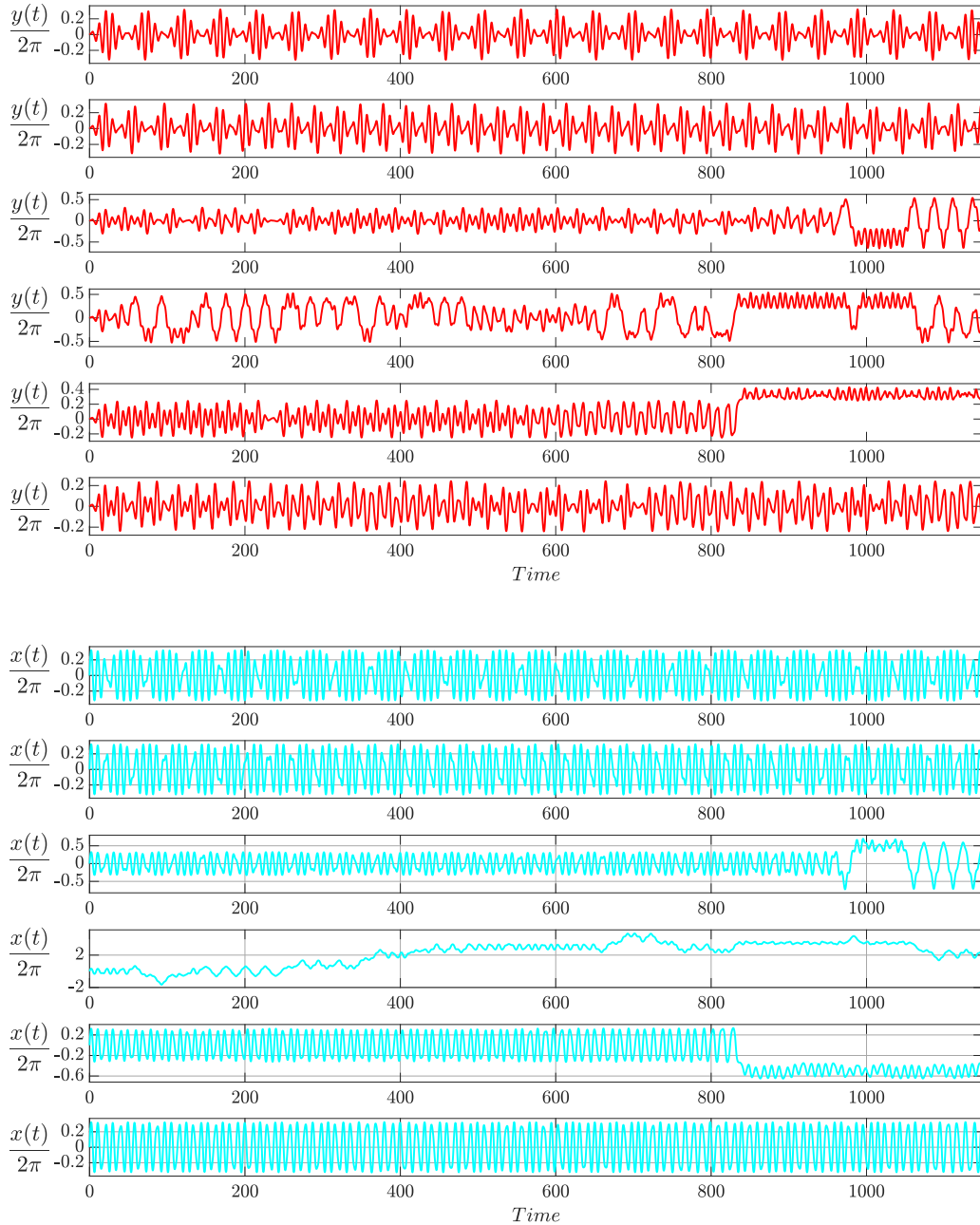


FIG. 13. Trajectories of the RC (upper panel, red) and the center of mass (lower panel, cyan) at the vicinity and in the *jumping* regime for $\epsilon = 0.85$ (corresponding to the energy E_0' in Fig. 5). From top to bottom in each panel: $K_1 = 0.10 K_S(\epsilon)$; $K_2 = 0.20 K_S(\epsilon)$; $K_3 = 0.33 K_S(\epsilon)$; $K_4 = 0.66 K_S(\epsilon)$; $K_5 = 0.99 K_S(\epsilon)$; $K_6 = 1.05 K_S(\epsilon)$.

surprising since we could imagine that, for a given energy, this access to the critical points could be facilitated by the increase the y amplitude for small stiffness as it is the case for smaller energy (see Fig. 9). Nevertheless, the main behavior observed on both sides of this jumping regime (K_1 and K_2 on the left side, K_6 on the right side) look like those observed at lower energy, as shown in Fig. 13.

These results suggest that the energetic condition is not sufficient and that there are dynamical constraints which forbid x and y to satisfy simultaneously the conditions required to reach the saddle point.

When $E_0/4U_0 > 1$, the jumps consist of a nonmonotonic motion of the center of mass, with a RC motion that does

not extend on more than a period of the external potential. In Sec. V, we have described the parametric amplification of the RC oscillations by the center-of-mass motion of a sliding dimer. A very good agreement was found for $\epsilon^{-1} = 0.4$, which is not a very small value. Nevertheless, we must insist on the fact that this is equivalent to $E_0/4U_0 \approx 6.25$, which means that the sliding regime described in Sec. V is outside the energy range of the behavior map in Fig. 5. In what follows, we focus on the range $1 \leq E_0/4U_0 \leq 2$ in connection with the Fig. 5, so that the perturbation parameter ϵ^{-1} ranges in $[1/\sqrt{2}, 1]$.

Let us first consider the transition line $K_f^>(\epsilon^{-1})$. In the energy range of Fig. 5, it separates a parametrically stable RC

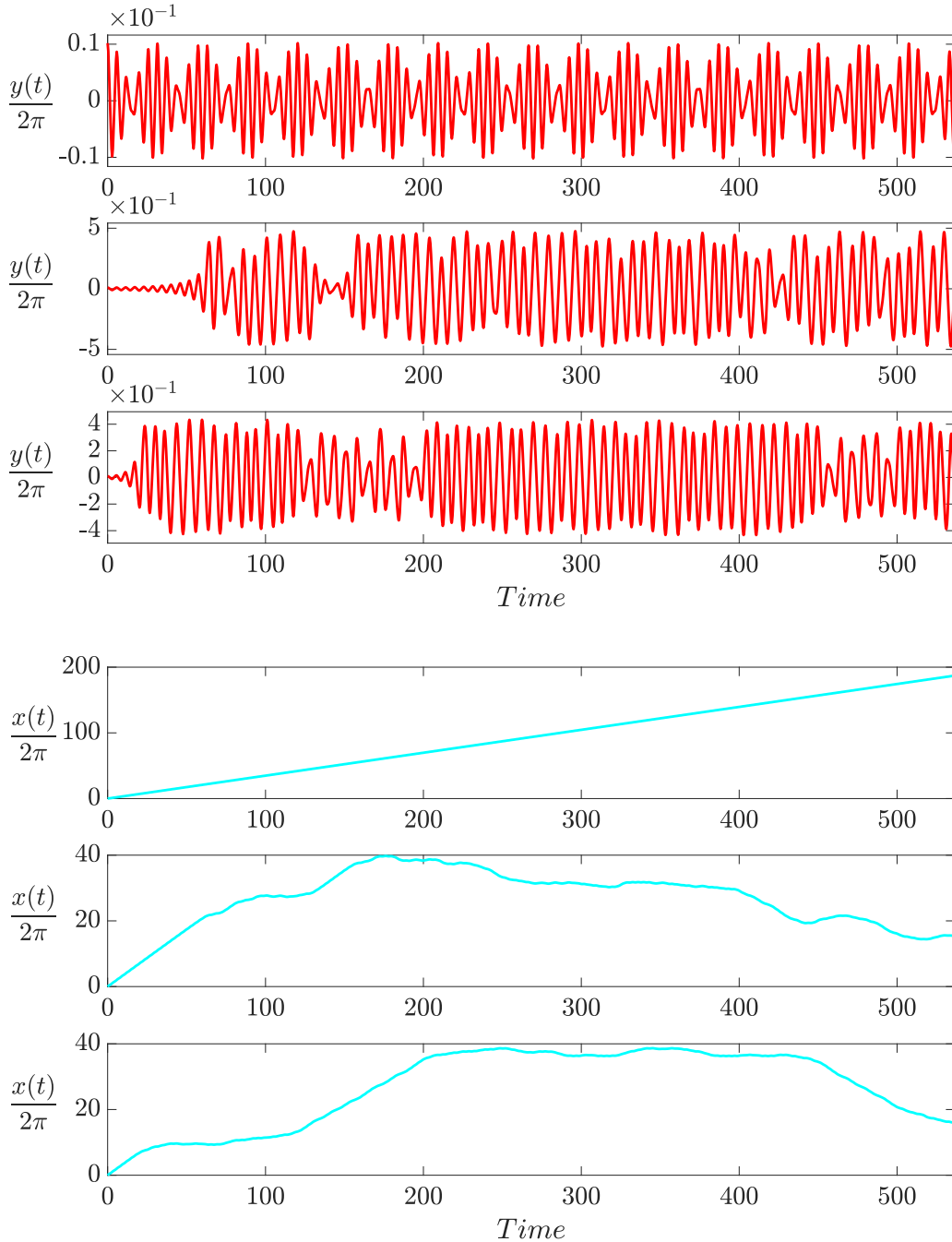


FIG. 14. Trajectories of the RC (upper panel) and the center of mass (lower panel) at the vicinity and in the *jumping* regime for $\epsilon^{-1} = 0.75$ and $\psi_0 = 0$ (corresponding to the energy E_0^{III} in Fig. 5). From top to bottom in each panel: $K_7 = 0.95K_J^<(\epsilon^{-1})$; $K_8 = 1.01K_J^<(\epsilon^{-1})$; $K_9 = 1.2K_J^<(\epsilon^{-1})$. Note that the saturation of the RC amplitude and the first deviation of the center of mass from a monotonic trajectory for K_8 and K_9 take place at the same time.

motion for $K < K_J^>(\epsilon^{-1})$ from a jumping regime. This is at odds with the perturbation expansion, which is not surprising since ϵ^{-1} is not small. This is illustrated in Fig. 14, where we plot $y(t)$ and $x(t)$ for a constant initial energy E_0^{III} an increasing values of the stiffness, $K_7 < K_8 < K_9$. For the first point, $K_7 < K_J^>(\epsilon^{-1})$, and the dimer motion is consistently stable since the stiffness is below the parametric instability threshold. For the two other points, the stiffness is above this threshold, and the dimer motion are in the jumping regime,

with a nonmonotonous motion of the center of mass. For the dimer with stiffness K_8 , which is only slightly above the parametric instability threshold, we clearly see an exponential increase of the RC amplitude at the beginning of the simulation.

Last, let us consider the transition line $K_J^<(\epsilon^{-1})$ in Fig. 5 for $E_0/4U_0 > 1$. The expansion parameter ϵ^{-1} is larger than 0.85, so that a poor agreement with the analysis that assumes $\epsilon^{-1} \ll 1$ is not surprising. Our automatic detection process

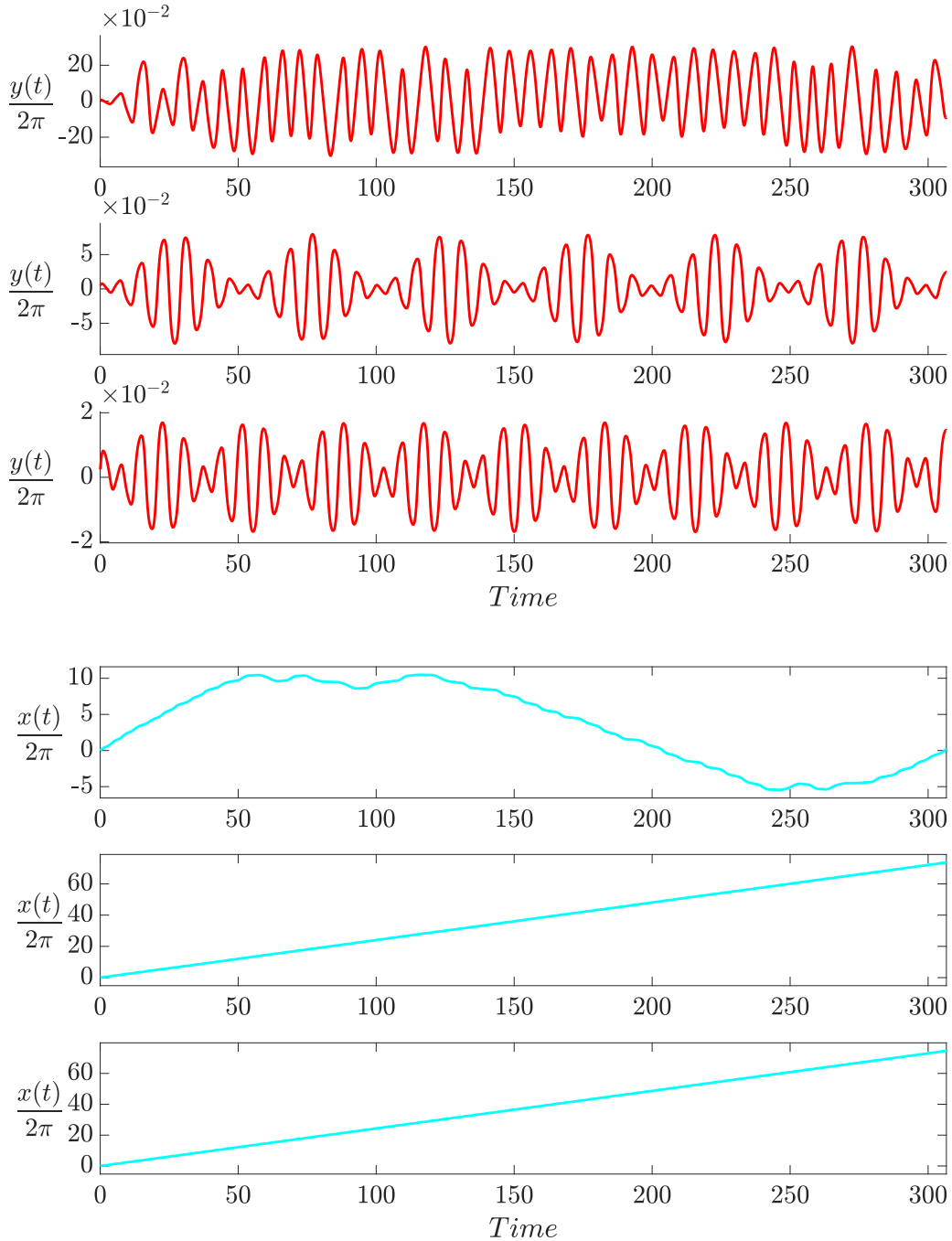


FIG. 15. Trajectories of the RC (upper panel) and the center of mass (lower panel) at the vicinity and in the *jumping* regime for $\epsilon^{-1} = 0.9$ (corresponding to the energy E_0^{II} in Fig. 5). The initial energy of the RC motion is $10^{-3}E_0^{II}$ and is randomly distributed between a kinetic part and a potential part. From top to bottom in each panel: $K_{10} = 0.800 K_I^+(\epsilon^{-1})$, $K_{11} = 0.975 K_I^+(\epsilon^{-1})$, and $K_{12} = 1.025 K_I^+(\epsilon^{-1})$.

(see Appendix C) predicts a somewhat blurred limit between dimers in a jumping regime and dimers in a stable sliding regime. This is confirmed by the plots of the relevant trajectories displayed in Fig. 15. We fix an initial energy E_0^{II} such that $\epsilon^{-1} = 0.90$ and choose increasing stiffnesses from K_{10} to K_{12} . For the stiffness K_{10} the dimer motion are fully consistent with a jumping regime. In contrast, for K_{11} and K_{12} the dimer motion is such that the center-of-mass motion is a translation and the RC a small oscillatory motion, that is a stable sliding motion of the dimer.

VII. CONCLUSION

A dimer in a periodic potential is a simple system with a complicated dynamics. It is conservative but not integrable. Its motion are determined by its initial energy and the stiffness of the interaction between the particles.

The systematic analysis of the dimer behavior through numerical simulations for a wide range of stiffness K and energy E_0 allows us to dress a global overview of the system although it is not necessary exhaustive. The numerical observations such as the exponential growth of the RC and

the merging of frequencies of the center of mass and RC evidence the parametric instability of the RC for a soft spring in the trapped configuration and a rigid spring in the sliding configuration. We also show that the theoretical predictions obtained within the frame of parameter ϵ such that $\epsilon \ll 1$ can be extended for higher values with a good agreement. In particular discrepancies may appear but the tendencies are preserved concerning the extrema amplitude and the period of the energy exchange in the trapped configuration. Moreover in both cases the instability boundaries seem to stay valid for ϵ up to 1, although for high values of ϵ the exponential amplification is distorted.

In the behavior map, a jumping domain is evidenced, for which the center of mass and RC follow irregular motions over several wells of the potential energy surface. This region is strongly related to the parametric instability domain since it requires a large deformation of the dimer to overcome the potential energy barrier given by the energy of the saddle points in the $E_0 < 4U_0$ configuration or to destabilize the center-of-mass trajectory in the $E_0 > 4U_0$ configuration. In particular the energetic analysis allows to delimit the jumping region in the $E_0 < 4U_0$ configuration. However, it is not sufficient since a domain in which the energetic analysis predicts a possible exit of the initial well is not subjected to jumping motion. This regular region is present for soft spring, in other words a region for which the curvature of the potential energy surface seen by the dimer is more homogeneous than for higher values of the stiffness.

APPENDIX A: EFFECTIVE MATHIEU EQUATION

The equations of motion of $x(t)$ and $y(t)$ can be considered as effective nonlinear Mathieu equations. Assuming that $|x(t)| \ll 1$ and $|y(t)| \ll 1$, and expanding the equations of motions [Eqs. (6) and (7)] up to third order, we get

$$\ddot{x} = -U_0x + \frac{U_0}{2}y^2x + \frac{U_0}{6}x^3, \quad (\text{A1})$$

$$\ddot{y} = -(2K + U_0)y + \frac{U_0}{6}y^3 + \frac{U_0}{2}yx^2. \quad (\text{A2})$$

If we inject the expressions of $x(t)$ and $y(t)$ from Eq. (11) in these equations, then we obtain

$$\ddot{x} + \Omega_x^2 \left[1 - \frac{\epsilon^2 b^2}{\Omega_x^2} \cos(2\Omega_y t + 2\psi) \right] x = 0, \quad (\text{A3})$$

$$\ddot{y} + \Omega_y^2 \left[1 - \frac{\epsilon^2 a^2}{\Omega_y^2} \cos(2\Omega_x t + 2\phi) \right] y = 0, \quad (\text{A4})$$

where

$$\Omega_x^2 = 1 - \epsilon^2 b^2 - \frac{\epsilon^2 a^2}{2}, \quad (\text{A5})$$

$$\Omega_y^2 = 2K + 1 - \epsilon^2 a^2 - \frac{\epsilon^2 b^2}{2}, \quad (\text{A6})$$

Physically, Eq. (A4) describes the parametric forcing of the RC by the center-of-mass motion, with a forcing amplitude $h = -\epsilon^2 a^2 / \Omega_y^2$ and a frequency $2\Omega_x$.

The condition to observe the main parametric resonance is [22],

$$1 - \frac{h}{4} \leq \frac{\Omega_x}{\Omega_y} \leq 1 + \frac{h}{4}. \quad (\text{A7})$$

In Fig. 7, the amplitudes a and b are found to be slowly varying functions of time, as well as the parameters h , Ω_x , and Ω_y . Let us assume that initial state of the system is such that the forcing h is in the instability tongue of the Mathieu equation. When the time goes on, instantaneous values of the parameters h , Ω_x , and Ω_y may be calculated if we inject the instantaneous values of the amplitudes a and b from the simulations data in Eqs. (A5) and (A6). These calculations give the representative points of the system in the plane $(\Omega_y/\Omega_x, h)$ displayed in the bottom plot of Fig. 7. This plot evidences that when the initial parameters of the system satisfy the parametric instability condition (A7), then this condition remains satisfied for ever.

Another interesting point is that the RC reaches its maximal amplitude when the system is on the instability boundary. By introducing the extrema values of a and b given by Eq. (17), $\epsilon^2 a_{\min}^2 = 2K$, $\epsilon^2 b_{\max}^2 = E_0/4U_0 - 2K$, and $U_0 = 1$, the frequencies are then:

$$\Omega_x^2 = \Omega_y^2 - E_0/8, \quad \Omega_y^2 = 1 + 2K - E_0/8. \quad (\text{A8})$$

This leads to the ratio $\Omega_x/\Omega_y = 1 - E_0/16\Omega_y^2 = 1 - (\epsilon a_0)^2/4\Omega_y^2$ which corresponds to the condition associated to the instability boundary $1 - h/4$.

APPENDIX B: PARAMETRIC AMPLIFICATION IN THE SLIDING REGIME

In this Appendix, we exhibit the link between our system and the theoretical analysis of Refs. [18,19]. It is reasonable to assume a very small relative displacement $|y(t)| \ll 1$, so that Eq. (7) now reads

$$\ddot{y} = -2Ky - U_0 \cos x \left(y - \frac{y^3}{6} \right), \quad (\text{B1})$$

valid up to order y^3 . The relevant expression of the coordinate $x(t)$ in the sliding regime is Eq. (15). At leading order, it gives

$$\ddot{y} = -[2K + U_0 \cos(V_0 t)]y + \frac{U_0}{6} \cos(V_0 t)y^3. \quad (\text{B2})$$

If we neglect the cubic term y^3 , then we recover a Mathieu equation describing the parametric amplification of y with a forcing frequency $V_0/2$, from which we get the instability threshold

$$U_0 \geq 2|2K - U_0/2E_0 - V_0^2|. \quad (\text{B3})$$

When $E_0 \gg U_0$ we obtain, as expected, $E_0 > 8K > E_0 - 4U_0$.

It has been shown in Refs. [18,19] that the coupling of the parametric excitation with the cubic term induces a parametric amplification of $y(t)$ when the basic frequency of the RC $\sqrt{2K} = V_0/4$. In the Supplemental Material of this paper [20], we display some trajectories $y(t)$ as a function of time that evidence a parametric amplification. Moreover, the relevant Fourier spectra evidence that the characteristic frequency of the RC, when it is parametrically amplified, is $V_0/4$.

APPENDIX C: MAP LAYOUT

In this section we give more details on the establishment of the behavior map. To each simulation point that makes up the map, we assign one of three labels: *parametrically stable*, *parametrically unstable*, or *jumping*. We first verify if we are facing a jumping motion; if not, then we evaluate if the motion is parametrically stable or unstable.

Concerning the jumping regime, the labeling process depends on whether we are at $E_0 < 4U_0$ or $E_0 > 4U_0$. When $E_0 < 4U_0$, the jumping regime is characterized by a time T_j such that the center-of-mass position $|x(T_j)|$ gets out its initial potential well. If we identify a time T_j in the simulations data (which means that it is less than the duration of a simulation), then the corresponding simulation is qualified as jumping.

When $E_0 > 4U_0$, this simple method becomes inefficient because the center of mass never stays in a potential well. The characteristic features of the jumping regime in this case are a nonmonotonic behavior of the center-of-mass coordinate, and an erratic motion of the RC. In practice, it is convenient to use this erratic motion of the RC to include a given simulation in the jumping regime. To this aim, we choose somewhat arbitrarily a critical value $y_c = \pi/2$ and we build a

symbolic trajectory $y_d(t)$ such as $y_d(t) = 0$ if $|y(t)|/y_c < 1/2$ and $y_d(t) = 1$ if $|y(t)|/y_c \geq 1/2$. In the symbolic trajectory, we record the indices that corresponds to changes from 0 to 1 and calculate the differences between successive indices. For a regular periodic motion, there are only a few distinct differences. In contrast, if the RC motion is erratic, then there is a much larger set of distinct differences between the indices. The search for abrupt changes was performed with the MATLAB built-in function `ischange`. This method is much quicker than trying to distinguish between a discrete (regular motion) and a continuous (erratic motion) frequency spectrum which is not numerically convenient. We confirm the relevance of this automatic process by plotting the full trajectories $\{x(t), y(t)\}$ in Figs. 13, 14, and 15.

If the simulation is not labeled as jumping, then the algorithm verifies whether it corresponds to stable or unstable motion of the RC. To this end, we consider the RC trajectory, we extract its envelope, and eventually we determine the initial variation of this envelope (i.e., the initial direction of the energy transfer between center of mass and RC). If the variation is negative, then the simulation corresponds to a parametrically stable situation; if it is positive, then it corresponds to an unstable situation.

-
- [1] A. S. Kovalev and A. I. Landau, Dynamical chaos and low-temperature surface diffusion of small adatom clusters, *Low Temp. Phys.* **28**, 423 (2002).
- [2] C. Fusco, A. Fasolino, and T. Janssen, Nonlinear dynamics of dimers on periodic substrates, *Eur. Phys. J. B Condens. Matter* **31**, 95 (2003).
- [3] M. Minkowski and M. A. Zaluska-Kotur, Diffusion of Cu adatoms and dimers on Cu(111) and Ag(111) surfaces, *Surf. Sci.* **642**, 22 (2015).
- [4] B. Denardo, J. Earwood, and V. Sazonova, Parametric instability of two coupled nonlinear oscillators, *Am. J. Phys.* **67**, 187 (1999).
- [5] R. Naz, I. Naem, and F. Mahomed, First integrals for two linearly coupled nonlinear Duffing oscillators, *Math. Prob. Eng.* **2011**, 831647 (2011).
- [6] S. Sabarathinam, K. Thamilmaran, L. Borkowski, P. Perlikowski, P. Brzeski, A. Stefanski, and T. Kapitaniak, Transient chaos in two coupled, dissipatively perturbed hamiltonian Duffing oscillators, *Commun. Nonlinear Sci. Numer. Simulat.* **18**, 3098 (2013).
- [7] S. Lenci, Exact solutions for coupled Duffing oscillators, *Mech. Syst. Sign. Process.* **165**, 108299 (2022).
- [8] S. V. Kuznetsov, The motion of the elastic pendulum, *Regul. Chaotic Dyn.* **4**, 3 (1999).
- [9] P. Lynch and C. Houghton, Pulsation and precession of the resonant swinging spring, *Physica D* **190**, 38 (2004).
- [10] M. A. Abramowicz, T. Bulik, M. Bursa, and W. Kluźniak, Evidence for a 2:3 resonance in Sco X-1 kHz QPOs, *Astron. Astrophys.* **404**, L21 (2003).
- [11] W. Kluźniak and M. A. Abramowicz, Resonant oscillations of accretion flow and kHz QPOs, *Astrophys. Space Sci.* **300**, 143 (2005).
- [12] J. Horak, The autoparametric 3:2 resonance in conservative systems, *Astron. Nachr.* **326**, 824 (2005).
- [13] J. Horak, Oscillations and Lightcurve Patterns of Accreting Black Holes, Ph.D. thesis, Charles University in Prague (2005).
- [14] E. Kartashova, *Nonlinear Resonance Analysis: Theory, Computation, Applications* (Cambridge University Press, Cambridge, UK, 2010).
- [15] J. Maddi, C. Coste, and M. Saint Jean, Parametric resonance in a conservative system of coupled nonlinear oscillators, *Phys. Rev. E* **105**, 054208 (2022).
- [16] In order to recast the results of Ref. [15], one has to note that the parameter K_2 used in our previous work has to be replaced here by $2K$.
- [17] W. H. Press, S. A. Teukolsky, W. T. Vetterling, and B. P. Flannery, *Numerical Recipes* (3rd. ed.) (Cambridge University Press, Cambridge, UK, 2007).
- [18] M. Mond, G. Cederbaum, P. Khan, and Y. Zarmi, Stability analysis of the non-linear Mathieu equation, *J. Sound Vib.* **167**, 77 (1993).
- [19] J. F. Rhoads, S. W. Shawa, K. L. Turner, J. Moehlis, B. E. DeMartini, and W. Zhang, Generalized parametric resonance in electrostatically actuated microelectromechanical oscillators, *J. Sound Vib.* **296**, 797 (2006).
- [20] See Supplemental Material at <http://link.aps.org/supplemental/10.1103/PhysRevE.106.064201> for RC trajectories and their Fourier transforms.
- [21] N. W. McLachlan, *Theory and Applications of Mathieu Functions* (Clarendon Press, Oxford, 1951).
- [22] L. Landau and E. Lifchitz, *Mécanique* (Mir Editions, Moscou, 1966).